AGU PUBLICATIONS

Geophysical Research Letters

RESEARCH LETTER
10.1002/2016GL067757

Key Points:
- Consistent changes to upper ocean circulation consistent with projected changes in surface winds
- Projected Indonesian Throughflow decrease related to deep ocean circulation
- Intermodel differences in upper circulation poorly described by Island Rule

Supporting Information:
- Supporting Information S1

Correspondence to:
A. Sen Gupta,
a.sengupta@unsw.edu.au

Citation:
Sen Gupta, A., S. McGregor, E. van Sebille, A. Ganachaud, J. N. Brown, and A. Santoso (2016), Future changes to the Indonesian Throughflow and Pacific circulation: The differing role of wind and deep circulation changes, *Geophys. Res. Lett.*, *43*, 1669–1678, doi:10.1002/2016GL067757.

Received 13 JAN 2016
Accepted 8 FEB 2016
Accepted article online 10 FEB 2016
Published online 29 FEB 2016

Future changes to the Indonesian Throughflow and Pacific circulation: The differing role of wind and deep circulation changes

Alex Sen Gupta[1], Shayne McGregor[2], Erik van Sebille[3], Alexandre Ganachaud[4], Jaclyn N. Brown[5], and Agus Santoso[1]

[1]Climate Change Research Centre and Australian Research Council (ARC) Centre of Excellence for Climate System Science, Mathews Building, University of New South Wales, Kensington, New South Wales, Australia, [2]School of Earth, Atmosphere and Environment, Monash University, Victoria, Australia, [3]Grantham Institute and Department of Physics, Imperial College London, London, UK, [4]LEGOS, Universtité de Toulouse, CNES, CNRS, IRD, UPS, France, [5]CSIRO, Hobart, Tasmania, Australia

Abstract Climate models consistently project a substantial decrease in the Indonesian Throughflow (ITF) in response to enhanced greenhouse warming. On interannual timescales ITF changes are largely related to tropical Pacific wind variability. However, on the multidecadal timescales investigated here we demonstrate that regional winds and associated changes in the upper ocean circulation cannot explain the projected ITF decrease. Instead, the decrease is related to a weakening in the northward flow of deep waters entering the Pacific basin at ~40°S and an associated reduction in the net basin-wide upwelling to the north of the southern tip of Australia. This can be traced back to consistent changes in the Antarctic Circumpolar Current and Southern Ocean overturning, although questions still remain as to the ultimate drivers. In contrast to the ITF decrease, substantial projected changes to the upper ocean circulation of the Pacific basin are well explained by robust changes in the surface winds.

1. Introduction

The subtropical Pacific Ocean circulation is dominated by two gyres. At their equatorial flanks flow the broad westward South and North Equatorial Currents that bifurcate along the continental margin forming the East Australian Current (EAC) and Gulf of Papua Current in the Southern Hemisphere and the Kuroshio and Mindanao Currents in the northern (Figure 1) [*Hu et al.*, 2015]. Unique to the Pacific basin is a tropical conduit, the Indonesian Throughflow (ITF), that allows water converging in the tropics, sourced largely from the Mindanao Current [*Wyrtki*, 1961] to escape from the Pacific into the Indian Ocean. A second westward escape route exists to the south of Australia via the EAC extension and the Tasman Leakage [*Van Sebille et al.*, 2012].

The ITF transports about 15 Sverdrup (Sv) of warmer and fresher Pacific water into the Indian Ocean with substantial variability across a range of timescales [*Sprintall et al.*, 2009; *Gordon et al.*, 2010]. Numerical simulations [*Hirst and Godfrey*, 1993; *Murtugudde et al.*, 1998; *Lee et al.*, 2002; *Song et al.*, 2007; *McCreary et al.*, 2007; *Santoso et al.*, 2011; *Le Bars et al.*, 2013] consistently demonstrate a major climate impact of the ITF, with the connection acting to cool the upper tropical Pacific and warm the surface Indian Ocean. It also affects the mean circulation, reducing the strength of the EAC and intensifying the Indian to Atlantic leakage via the Agulhas current [e.g., *Le Bars et al.*, 2013]. In addition, the ITF can significantly modulate Indo-Pacific interannual variability [*Song et al.*, 2007; *Koch-Larrouy et al.*, 2009; *Santoso et al.*, 2011; *Yuan et al.*, 2012] and regional biogeochemistry [*Ayers et al.*, 2014]. Recently, it has also been suggested that the ITF also plays a role in the dynamics of the global warming hiatus [e.g., *England et al.*, 2014] through the redistribution of the excess heat stored in the tropical Pacific into the Indian Ocean [*Lee et al.*, 2015]. The ITF is thus an important part of the climate system and any future changes will have important ramifications for regional and global climate variability and change (see also review by *Sprintall et al.* [2014]).

The mean ITF is maintained by a pressure difference between the Pacific and Indian basins. Both mean flow and its variability are modulated by both local and large-scale Indo-Pacific winds. In particular, tropical wind variability associated with the El Niño—Southern Oscillation, Indian Ocean variability [*Meyers*, 1996; *Murtugudde et al.*, 1998; *Masumoto*, 2002; *England and Huang*, 2005], and local monsoonal winds [*Gordon et al.*, 2003; *Susanto et al.*, 2007] are important drivers of ITF transport change. Most notably stronger (weaker) Pacific trade winds during La Niña (El Niño) conditions act to strengthen (weaken) the upper ITF [*Meyers*, 1996; *England and*

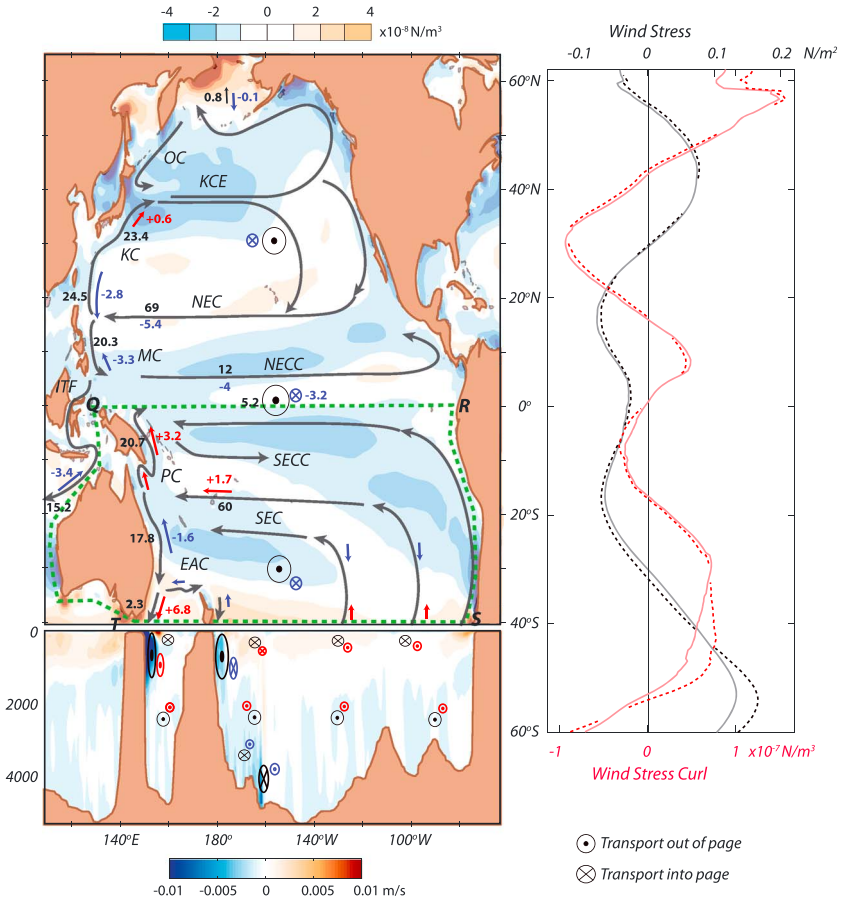

Figure 1. (left) Schematic of major currents (black lines with arrows indicating the mean direction), projected change in wind stress curl (upper panel contours), and projected change in meridional velocity (lower panel contours at 40°S); mean transports (Sv) are shown in black numbers with red (blue) numbers indicating a projected MMM increase (decrease) in current transport. Size of symbols indicating transport in/out of page is indicative of current or current anomaly magnitude. (right) The multi-model mean zonally averaged (Pacific Basin) zonal wind stress (black) and wind stress curl (red) for twentieth century (solid) and 21st century (2050–2100; dashed; only shown where the mean change is significant at 95% level based on a student *t* test).

Huang, 2005; *Sprintall and Révelard*, 2014; *Van Sebille et al.*, 2014]. While interannual and shorter-term variability has been linked to changes in tropical Pacific winds, on longer timescales ITF variability has been related to extratropical influences via changes to the subtropical cells [*Valsala et al.*, 2011].

Our primary focus here is to understand the projected changes to the ITF resulting from future increases in greenhouse gases. Since the ITF forms an integral part of the large-scale Pacific Ocean circulation, it is relevant to also examine the other major currents in the region. On multidecadal timescales, where oceanic adjustment results in quasi steady state conditions, Sverdrup and Island Rule [*Godfrey*, 1989] dynamics have been used to explain projected circulation changes [e.g., *Cai et al.*, 2005; *Sen Gupta et al.*, 2012; *Oliver and Holbrook*, 2014]. Previous studies have identified a projected weakening of the ITF and significant changes to the Pacific current system [e.g., *Cai et al.*, 2010; *Ganachaud et al.*, 2012; *Sen Gupta et al.*, 2012; *Hu et al.*, 2015]. In particular, *Hu et al.* [2015] noted that the ITF weakening could be related to deep circulation changes, although the mechanisms behind this projected change were not examined. We address this issue by diagnosing circulation changes in terms of a simplified linear barotropic description of circulation. Evaluating the validity of these theoretical frameworks in explaining the projected changes provides insight into the underlying mechanisms.

2. Climate Models

We use output from 33 CMIP5 climate models (Table S1 in the supporting information) and consider two CMIP5 experiments: (i) the *historical* simulations, which utilize observationally derived external forcing and

(ii) the RCP8.5 scenario [*Moss et al*., 2010] in which atmospheric greenhouse gas emissions remain unabated over the 21st century reaching CO2-equivalent concentrations of ~1370 ppm in 2100. Not all of the models have the complete set of variables needed to calculate all metrics described in this study (Table S2). Consistent models and model realizations are selected when comparing the relationship between different variables. To minimize any influence of low frequency variability in projected changes, averages over two long time periods are considered: 1900–2000 from the historical simulations and 2050–2100 from RCP8.5. The multidecadal timescale considered here provides sufficient time for the ocean circulation to adjust to changes in surface forcing.

3. Transport and Island Rule Calculation

Models have very different coastlines and bathymetry. As such, the pathway and widths of currents can vary considerably (e.g., Figure S1). Consequently, the domain used to define different currents and the Island Rule integration pathways were manually identified for each model. The eastern extents of the western boundary currents are selected so as to include the core of the current and any associated weak offshore counter current (which is often present, see example in Figure S1). Results are insensitive to the exact longitude of the eastern boundary as long as it encompasses the strong western boundary core. The upper ocean wind-driven circulation in particular the western boundary currents are largely confined above 2000 m in the models. Upper ocean transport between the eastern edge of the western boundary current and the American coastline constitute the *interior* circulation. ITF transport is defined as the full depth net transport entering the Indian Ocean at about 114°E, between the northern tip of Australia and the southern tip of Asia.

The efficacy of the Island Rule (see supporting information for detailed description) was tested in a 1 1/2 layer shallow water model (SWM) [*McGregor et al*., 2007] forced by the projected changes in wind stress from 21 CMIP5 models. By model design there is no circulation change in the deep ocean. We find a strong intermodel relationship between the change in SWM ITF transport (or upper basin-wide flow east of Australia) and the Island Rule-derived transport (Figure S7) with a correlation of 0.7 (0.9). Moreover the magnitudes of changes are similar between ITF, basinwide northward flow (to the east of Australia), and Island Rule transport.

4. Projected Circulation Changes

4.1. Southern Hemisphere

The models consistently project substantial changes across the Pacific under a business as usual increase in greenhouse gas concentrations. Some of these changes have been described in *Hu et al*. [2015]. In this section we extend this analysis, providing greater quantification and information on additional circulation features. One of the most dramatic changes is an intensification of the southward flowing EAC extension, south of ~29°S. Indeed, a strong intensification of the EAC extension has been observed over recent decades [*Roemmich et al*., 2007; *Hill et al*., 2008; *Cetina-Heredia et al*., 2014]. All the models project an intensification with a multimodel mean (MMM) increase of 6.8 Sv averaged between 35 and 45°S (range ~2 Sv to ~13 Sv; see Table S2 for transport values for all models and the associated changes). This consistent increase occurs despite very different twentieth century mean transports in the extension region; indeed 5 of 22 models have a net northward transport. The MMM EAC extension transport is −2.3 Sv (range −15 Sv to +11 Sv; Table S2). Those models exhibiting a spurious northward transport unrealistically exhibit a full separation of the EAC flow at around 30°S toward the east (Figures S2a and S2b). These models have distinct wind fields compared to those with a realistic southward transport. In particular, the maximum midlatitude westerlies sit too far north. As a result, the positive wind stress curl located to the east of Australia decreases prematurely southward of 30–35°S (Figures S2c and S2d). Interestingly, there is a significant negative correlation between mean state and projected change in transport for the EAC extension ($r = -0.6$, $p < 0.01$), i.e., models with weak or northward transport project the largest future intensification. This suggests that the more moderate estimates of future intensification may be more plausible.

At lower latitudes, there is a slight weakening in the southward western boundary flow to the north of the EAC maximum in most (17 out of 22) models with a MMM reduction of 1.6 Sv from the 17.8 Sv twentieth century mean, averaged between 20 and 30°S ($p < 0.01$, based on a student t test). At the EAC maximum itself (calculated for each model individually), the sign of the projected transport change is not consistent across

the models. However, all models project a southward shift in the latitude of the maximum, with a MMM shift of 0.7° (range 0.25° to 1.75°) from a twentieth century MMM latitude of about 28°S (Table S2).

Farther north, the northward flowing Gulf of Papua Current (including the North Queensland and Great Barrier Reef currents; SPICE Community 2012) is projected to increase in most (18/22) models by a MMM of 1.9 Sv (averaged between 12.5 and 17.5°S, Table S2) from a twentieth century mean of 15 Sv. This is associated with a SEC intensification of 1.9 Sv (at 170°E). Indeed, a strong intermodel relationship exists between the projected SEC and the Gulf of Papua Current minus the Northern EAC (20–25°S) transport changes ($r = 0.75$, $p < 0.01$). In the tropics, the New Guinea Coastal Undercurrent (NGCU) is also projected to increase (MMM of 3.2 Sv) in all but one model, from 20 Sv. A robust NGCU intensification was identified in the CMIP3 models related to a strong projected change in the wind stress curl across the basin just south of the equator [*Sen Gupta et al*., 2012], associated with a robust intensification of the southeasterly trade winds and reduction in the equatorial easterly winds. *Sen Gupta et al*. [2012] linked the NGCU intensification to an increase in Equatorial Undercurrent (EUC) strength across the western and central Pacific. A similar wind stress curl change is evident in the CMIP5 models (Figure 1). We also find an EUC intensification in the multimodel mean (3.0 Sv from a 44 Sv twentieth century mean, at 170°E, Table S2); however, model agreement on the sign of change is poor, with only 14 of 22 models projecting an increase.

4.2. Northern Hemisphere

In the Northern Hemisphere, most models (19/22) project a decrease in the strength of the Mindanao Current (2.9 Sv from 21 Sv, averaged between 5 and 10°N). Again this is consistent with the CMIP3 models (although model agreement was poorer for CMIP3). This was related to wind stress curl changes resulting from a robust weakening of the north easterly trade winds [*Sen Gupta et al*., 2012, their Figure 3].

To the north, the models consistently project a decrease at, and to the south, of the Kuroshio Current maximum. Between 15 and 25°S, 21 of 22 models show a decrease in transport with a MMM decrease of 2.7 Sv (Table S1, from 24.5 Sv). A similar multimodel mean decrease is projected for the maximum transport; however, most models project little change in the maximum latitude. North of this latitude, models do not agree on the sign of the Kuroshio Current change.

The changes to the Mindanao and southern Kuroshio currents are associated with a reduction in the eastward transport of the North Equatorial Counter Current (NECC, which reduces by 5.4 Sv from 69 Sv at 170°E, MMM). A strong intermodel correlation exists between the change in NECC transport and the change in the divergence of the Mindanao and Kuroshio Currents ($r = 0.9$. $p < 0.01$).

4.3. Indonesian Throughflow

The MMM ITF transport into the Indian Ocean is 15.2 Sv (Figure 2a and Table S2) with a relatively small intermodel range (11 to 20 Sv). This is in remarkable agreement with observational estimates (15 Sv) [*Sprintall et al*., 2009] despite the poor representation of the Indonesian Archipelago in the models. This may reflect some degree of bathymetric adjustment and tuning of parameters, given the importance of this oceanic choke point.

All of the models project a reduction in the ITF strength by ~1 to 6 Sv, with a MMM reduction of 3.4 Sv (Figure 2a), corresponding to over 20%. This change is large compared to interannual fluctuations in the simulated ITF transport: based on a subset of models, the projected change generally exceeds 3 standard deviations of annual ITF transport fluctuations (annual ITF standard deviation ranges between ~0.5 and 1.5 Sv, Figure 2a).

Sen Gupta et al. [2012] suggested that the ITF reduction in the CMIP3 models might result from a weaker Mindanao Current transport given that the changes in the two transports have similar magnitudes and the Mindanao Current is thought to be a primary source for the ITF [e.g., *Wyrtki*, 1961]. In the CMIP5 models, the MMM ITF and Mindanao Current reductions are also similar (Table S2). However, no significant intermodel relationship exists between these metrics (nor is there a relationship between mean twentieth century Mindanao Current and ITF transport $|r| < 0.1$).

4.4. Drivers of Change

The CMIP5 models project robust changes to Pacific winds. In particular, there is a southward intensification of the midlatitude westerlies centered around 50°S [e.g., *Swart and Fyfe*, 2012], an intensification of the

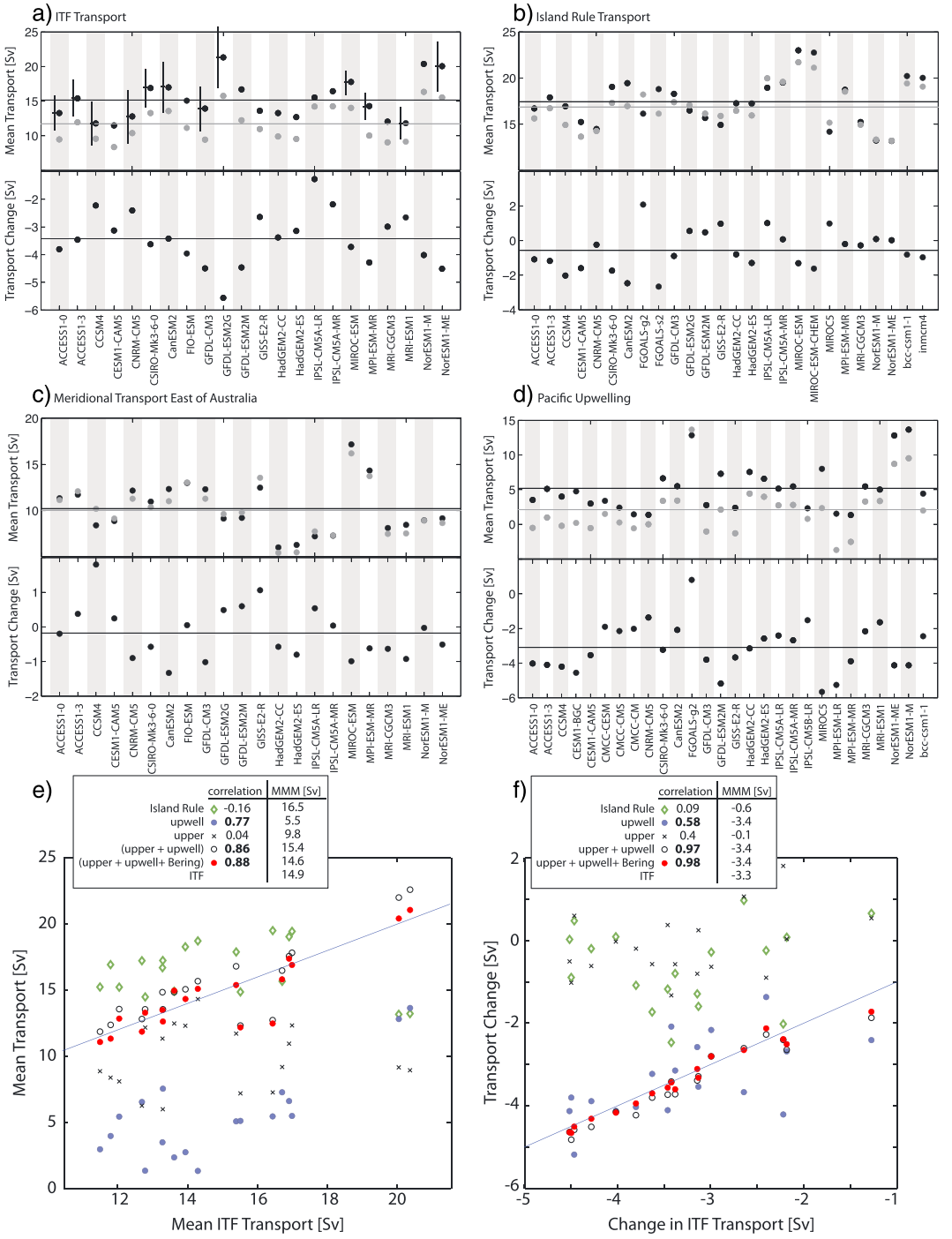

Figure 2. (a) Long-term mean 1900–2000 (black) and 2050–2100 (grey) ITF (upper panel) and associated change (lower panel), (b) as Figure 2a for Island Rule Transport, (c) as Figure 2a for upper ocean (<2000 m) meridional transport east of Australia at 38°S, (d) as Figure 2a for upwelling across 2000 m. Horizontal lines indicate multimodel means, vertical black lines in Figure 2a indicate interannual annual ITF variance (3x standard deviation based on combined historical and RCP85 data with 100 year loess filtered data removed, to retain interannual component of variability). (e) Relationship between ITF transport and (i) Island Rule upper ocean northward transport, (ii) modeled upwelling, (iii) modeled upper ocean northward transport, (iv) ii + iii, and (v) ii + iii + Bering Strait transport; associated correlations and multimodel mean transports shown in inset. (f) as Figure 2e for transport change. Note transport change values differ slightly from those in Table S2 as they represent the average across the subset of models for which both wind and transport data are available.

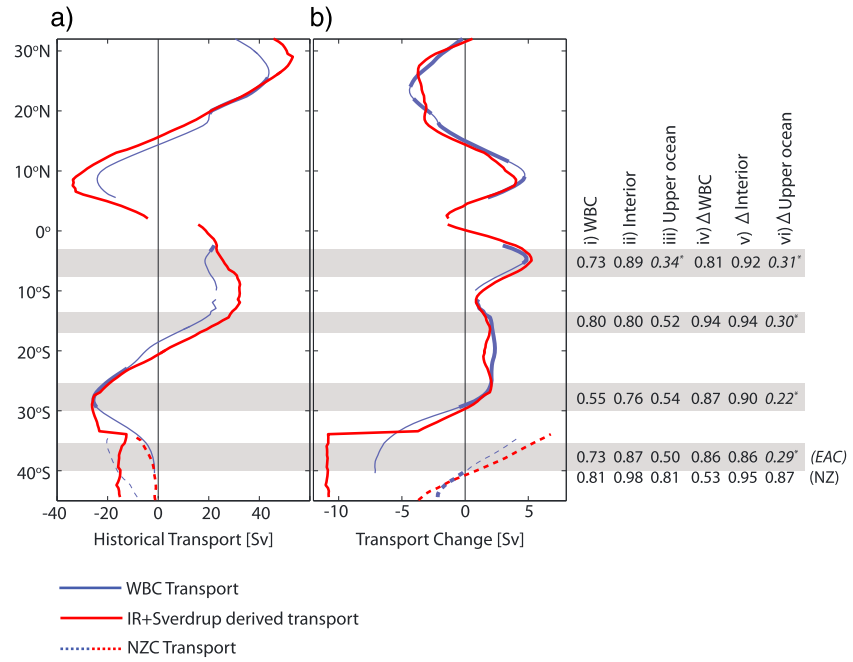

Figure 3. Multimodel (a) mean and (b) projected change in western boundary current transport (blue) and wind-derived transport using Sverdrup and Island Rule calculations (red) (see supporting information). Western boundary transport to the east of New Zealand is also shown (dashed). Transport lines (blue) are thickened where multimodel mean transport and wind-derived transport estimates are indistinguishable at the 95% level (based on a student *t* test). Numbers shown on the right are intermodel correlation between model and wind-derived (IR and Sv) transport for (i) western boundary currents, (ii) interior transport, (iii) total upper ocean northward basin transport (in the upper 2000 m), and (iv–vi)projected changes in these transports, averaged over the latitude bands marked in grey. All correlations except those marked with an asterisk are significant at the 95% level.

southeasterly trade winds and a weakening of equatorial and northeasterly trade winds (Figure S5). This in turn results in significant changes in the Pacific wind stress curl (Figure 1).

Figure 3a shows the implied western boundary current transport related to purely wind-driven changes, based on Sverdrup and Island Rule estimates [*Godfrey*, 1989] (see supporting information for further explanation). Latitudinal variations in boundary transport strength are well reproduced by the wind-derived estimates. However, these estimates are generally too large in magnitude; in particular there are large systematic biases in the EAC extension region to the south of 29°S. Here wind-derived estimates of the western boundary transport are much larger than actual model transports. Conversely, wind-derived estimates are systematically too small for the boundary current east of New Zealand. For all the latitude bands shown, there is a strong relationship between model interior transports and the associated Sverdrup estimates (intermodel correlations range $r = 0.76$ to 0.98, Figure 3a). Conversely, the relationship between modeled and Island Rule-derived net upper ocean meridional transports to the east of Australia is considerably poorer ($r < 0.54$) and at some latitudes not statistically significant. As such the moderate correlations between wind-derived and simulated western boundary current transport largely stem from the efficacy of the Sverdrup relation. Unlike the full basin transport, intermodel differences in meridional transport to the east of New Zealand are strongly correlated with the Island Rule estimate ($r = 0.81$) despite a large systematic bias in the magnitude of the wind-derived estimates.

Differences in projected changes in the western boundary currents are also well explained by changes in the wind fields ($r > 0.81$ for all regions). However, the efficacy of this again primarily stems from accurate Sverdrup-derived estimates of interior transport change (intermodel correlations > 0.87); the upper ocean basinwide transport changes east of Australia do not agree well with the Island Rule-derived changes (nonsignificant intermodel correlations; Figure 3b). These correlations would become significant ($r > 0.59$, $p < 0.05$) if an outlier model (CCSM4) is neglected; however, we have no good justification for neglecting this model. Despite a poor intermodel relationship, both simulated and Island Rule-derived net upper ocean

transport changes indicate a small <5% weakening (−0.2 and −0.6 Sv, respectively, in the MMM; Table S2). Within the Island Rule framework, these values should roughly match the change in the ITF. However, the MMM ITF change (~3 Sv) is about 22% of its twentieth century mean value, far greater than can be explained by purely wind-derived estimates. In some models the net upper ocean meridional transport change could constitute a larger contribution to the ITF change (>25% for four of the models). However, this is not the case for the majority of models. Thus, the ITF change must be primarily related to factors other than changes in regional winds and upper ocean circulation, in particular deep circulation changes must be important.

To examine deep circulation changes, we calculate net upward transport of water at 2000 m integrated over the basin to the north of ~40°S (Figure 2d; upwelling across 2000 m is presented instead of the equivalent net deep flow into the Pacific at 40°S, as more model output was available for the former variable). All models ($n = 28$, Table S2) exhibit a net twentieth century mean upwelling of water in the Pacific Basin north of ~40°S, with a MMM upwelling of 5.2 Sv (range 1.3 to 13.7 Sv; Table S2). While this only potentially constitutes 1/3 of the mean ITF transport, a significant correlation exists between the mean twentieth century upwelling and mean ITF transport across the common models ($r = 0.77$, $p < 0.01$; Figure 2e) suggesting that a substantial fraction of the model diversity in the mean ITF transport results from differences in the deep circulation.

In all models, except FGOALS-g2, upwelling is projected to decrease, with a MMM reduction of 3.1 Sv (3.3 Sv for 19 common models with ITF data; Figure 2d). Interestingly in some (8/28) models this results in a net downwelling of water at 2000 m in the Pacific Basin for the 2050–2100 period or equivalently a net transport out of the deep Pacific at 40°S. Examination of spatial maps of upwelling (not shown) indicates that the decrease in upwelling occurs throughout the basin and is not associated with particular regions or topographical features. These projected changes can be traced to a basin-wide reduction in the net northward flow entering the Pacific basin below 2000 m (Figures 1 and S3). The largest change is associated with a reduction in bottom water entering the Pacific along the eastern flank of the New Zealand continental shelf. The MMM projected decrease in upwelling closely mirrors the decrease in the ITF (~3.3 Sv) with a significant correlation of $r = 0.6$ ($p < 0.01$; Figure 2f). As expected the correlation approaches unity if the upper ocean meridional changes to the east of Australia are also considered (Figure 2f), i.e., upper ocean changes are still important to understand the diversity in model ITF projections, even though the MMM change is small.

Other potential factors affecting ITF transport include changes to the Bering Strait transport and net precipitation (for those models where ocean volume can change). All models except GISS-E2-R have a net northward twentieth century Bering Straits transport, with MMM transport of 0.8 Sv (range −0.1 to 1.6 Sv, Table S2). This compares well with the observed northward transport of 0.83 Sv [*Roach et al.*, 1995]. In most (16/22) models, water exiting through the Bering Straits reduces in the future, with a MMM reduction of 0.13 Sv or 15% (range −0.9 to +0.05 Sv; Table S2).

There are significant changes in regional net precipitation with projected increases of ~1 mm/d in the equatorial region and smaller decreases at subtropical latitudes (Figure S4) consistent with an intensification of the hydrological cycle [*Levang and Schmitt*, 2015]. However, these changes largely compensate each other over the Pacific basin resulting in a MMM increased flux of water into the basin of only 0.03 Sv (Figure S4; with a range of −0.17 to 0.24 Sv). Thus, changes to both the Bering Strait transport and the hydrological cycle play only a minor role in the ITF change.

5. Discussion

Consistent changes to the Indo-Pacific winds are projected by the CMIP5 models, including a small relaxation of the equatorial trade winds (Figures 1 and S5). Given the significant interannual relationship between ITF transport and equatorial wind strength (with interannual correlations between ITF transport and eastern/central Pacific zonal winds ranging from 0.43 to 0.85 across models; Figure S6), one might expect a future ITF decrease. While a decrease is projected (~3.4 Sv MMM, equivalent to >20% change), the projected trade wind relaxation is far too small to be a major factor (Figure S6, filled circles).

Based on the Island Rule [*Godfrey*, 1989], we would expect winds over a larger domain to affect ITF transport on the timescales considered. Indeed, a shallow water ocean model (SWM) forced with wind stresses form selected CMIP5 models exhibits good agreement between Island Rule derived and SWM upper ocean basin-wide meridional transport. This is not the case for the CMIP5 models, however, where no significant

intermodel relationship is found between the Island Rule and associated model transports for projected changes (and only a weak relationship of the twentieth century mean circulation, Figure 3). This is possibly because the Island Rule estimate represents a small residual from large competing influences along the Island Rule path integral (Figure S5d). While there is no intermodel relationship, both basin-wide meridional transport and the associated Island Rule derived estimate both indicate a slight weakening (<5% of their twentieth century mean state values). However, this weakening is too small (MMM ~0.6 Sv) to explain the projected ITF reduction.

Instead, the projected ITF weakening appears to be largely related to deep circulation changes and a robust projected decrease in upwelling across the Pacific Basin at 2000 m. This reduced upwelling is equivalent in magnitude to the projected decrease in ITF, with a significant intermodel relationship (Figure 2f). These deep changes can be linked to Southern Ocean circulation changes. While there is little model agreement in the projected Antarctic Circumpolar Current transport changes in the CMIP5 [e.g., *Meijers*, 2014], there is unanimous agreement regarding a projected reduction in the net zonal convergence of water into the Pacific sector of the Southern Ocean (between 145°E and 290°E and south of 37°S, Figure S8a), consistent with the projected ITF reduction.

Interestingly, this reduction in zonal high-latitude convergence occurs in both the upper (above 2000 m) and lower ocean in almost all models, with a MMM decrease in convergence of between 1.5 and 2 Sv in both depth ranges (Figure S9a). At the same time, there is also a projected reduction in the mean downwelling (i.e., a net upward flux) at 2000 m in the Pacific sector of the Southern Ocean in almost all models (MMM decrease of 1.7S v, Figure S9b), which largely compensates the decreased upper ocean zonal convergence. This results in little projected change in the northward transport of water into the Pacific Basin in the upper ocean and a sizable reduction in the deep net northward transport that is consistent with the ITF transport change. While this reduction in northward transport occurs across the entire Pacific basin below ~2000 m (Figures 1 and S3b), the largest ensemble mean reduction is clearly seen in the region of bottom water transport to the east of New Zealand (Figure S3b). This is consistent with the global decrease in bottom water transport previously noted for both CMIP3 and CMIP5 [*Sen Gupta et al*., 2009; *Meijers*, 2014].

It should be remembered, however, that the fidelity of water masses in the CMIP5 models is poor, in particular the northward transport of bottom water is systematically underestimated [*Sallée et al*., 2013]. Regardless of this, our work raises interesting questions regarding the ultimate driver of the ITF changes. Sensitivity experiments could be used to isolate the relative roles of increased Pacific stratification (associated with surface warming), changes in the Southern Hemisphere westerlies and the reduction in high-latitude buoyancy in generating the circulation changes noted here. This will be the subject of future work

In the CMIP5 models, the close match between upwelling and ITF changes mean that changes to the Southern Hemisphere western boundary currents and upper ocean interior transport must largely compensate each other. This is indeed the case (Figures S8a and S8b), although south of the northern tip of New Zealand the situation is complicated by the presence of two boundary currents.

While the change in the projected basin-wide meridional transport is small, the equivalent change east of New Zealand is substantial (MMM 6.7 Sv, Table S2 and Figure S8e) and consistent with a large Island Rule derived increase (MMM 10.4 Sv, $r = 0.89$). In this case, all legs of the Island Rule path integral for New Zealand (Figure S4a) contribute positively to this increase. There is also an increase in the northward interior transport to the east of New Zealand that weakens toward the north, associated with a positive wind stress curl anomaly from enhanced midlatitude winds (Figure 1). In combination, this results in a decrease in the southward western boundary transport along northern New Zealand. The large projected increase in water entering the Pacific Basin east of New Zealand is instead largely compensated by the EAC extension intensification (Figure S8e).

6. Summary

Based on a simplified (linear barotropic) description of the surface circulation, we show that the projected changes in the wind should generate little change in the ITF transport. However, all the CMIP5 models project a substantive reduction. While changes in regional winds are important for ITF variability on shorter timescales, our results show that changes in the ITF on multidecadal timescales are primarily related to overturning

circulation changes. In the Pacific sector of the Southern Ocean there is a reduction in the zonal convergence of water (entering south of Australia and leaving through the Drake Passage) in both the upper and lower ocean (see Figure S10 for schematic of changes). There is also a consistent projected increase in upwelling, in this region, which compensates for the weaker zonal convergence in the upper layer but further reduces the net transport into the deep Pacific Southern Ocean. This results in weaker deep transport into the deep Pacific basin at the latitude of the southern tip of Australia, weaker Pacific upwelling, and ultimately a reduced ITF. The ultimate driver of these changes remains an open question.

Acknowledgments

For their roles in producing, coordinating, and making available CMIP5 model output, we acknowledge the climate modeling groups (Table S1), the World Climate Research Programme's Working Group on Coupled Modelling and the Global Organization for Earth System Science Portals. This work was supported by the Australian Research Council (ARC) including the ARC Centre of Excellence in Climate System Science and the NCI National Facility, Canberra. E.v.S. was supported by the ARC under grant DE130101336. S.M. was supported by the ARC under grant DE130100663. We would also like to thank the two anonymous reviewers for their useful feedback.

References

Ayers, J. M., P. G. Strutton, V. J. Coles, R. R. Hood, and R. J. Matear (2014), Indonesian throughflow nutrient fluxes and their potential impact on Indian Ocean productivity, *Geophys. Res. Lett.*, *41*, 5060–5067, doi:10.1002/2014GL060593.

Cai, W., G. Shi, T. Cowan, D. Bi, and J. Ribbe (2005), The response of the Southern Annular Mode, the East Australian Current, and the southern mid-latitude ocean circulation to global warming, *Geophys. Res. Lett.*, *32*, L23706, doi:10.1029/2005GL024701.

Cai, W., T. Cowan, S. Godfrey, and S. Wijffels (2010), Simulations of processes associated with the fast warming rate of the southern midlatitude ocean, *J. Clim.*, *23*, 197–206.

Cetina-Heredia, P., M. Roughan, E. van Sebille, and M. A. Coleman (2014), Long-term trends in the East Australian Current separation latitude and eddy driven transport, *J. Geophys. Res. Oceans*, *119*, 4351–4366, doi:10.1002/2014JC010071.

England, M. H., and F. Huang (2005), On the interannual variability of the Indonesian Throughflow and its linkage with ENSO, *J. Clim.*, *18*, 1435–1444.

England, M. H., S. McGregor, P. Spence, G. A. Meehl, A. Timmermann, W. Cai, A. S. Gupta, M. J. McPhaden, A. Purich, and A. Santoso (2014), Recent intensification of wind-driven circulation in the Pacific and the ongoing warming hiatus, *Nature Clim. Change*, *4*, 222–227, doi:10.1038/nclimate2106.

Ganachaud, A., A. Sen Gupta, J. N. Brown, K. Evans, C. Maes, L. C. Muir, and F. S. Graham (2012), Projected changes in the tropical Pacific Ocean of importance to tuna fisheries, *Clim. Change*, doi:10.1007/s10584-012-0631-1.

Godfrey, J. S. (1989), A Sverdrup model of the depth-integrated flow for the world ocean allowing for island circulations, *Geophys. Astrophys. Fluid Dyn.*, *45*, 89–112, doi:10.1080/03091928908208894.

Gordon, A. L., R. D. Susanto, and K. Vranes (2003), Cool Indonesian throughflow as a consequence of restricted surface layer flow, *Nature*, *425*, 824–828, doi:10.1038/nature02038.

Gordon, A. L., J. Sprintall, H. M. Van Aken, D. Susanto, S. Wijffels, R. Molcard, A. Ffield, W. Pranowog, and S. Wirasantosa (2010), The Indonesian throughflow during 2004–2006 as observed by the INSTANT program, *Dyn. Atmos. Oceans*, *50*, 115–128, doi:10.1016/j.dynatmoce.2009.12.002.

Hill, K., S. Rintoul, R. Coleman, and K. Ridgway (2008), Wind forced low frequency variability of the East Australia Current, *Geophys. Res. Lett.*, *35*, L08602, doi:10.1029/2007GL032912.

Hirst, A. C., and J. S. Godfrey (1993), The role of Indonesian Throughflow in a global ocean GCM, *J. Phys. Oceanogr.*, *23*, 1057–1086, doi:10.1175/1520-0485(1993)023<1057:TROITI>2.0.CO;2.

Hu, D., et al. (2015), Pacific western boundary currents and their roles in climate, *Nature*, *522*, 299–308, doi:10.1038/nature14504.

Koch-Larrouy, A., M. Lengaigne, P. Terray, G. Madec, and S. Masson (2009), Tidal mixing in the Indonesian Seas and its effect on the tropical climate system, *Clim. Dyn.*, *34*, 891–904, doi:10.1007/s00382-009-0642-4.

Le Bars, D., H. A. Dijkstra, and W. P. M. De Ruijter (2013), Impact of the Indonesian throughflow on Agulhas leakage, *Ocean Sci. Discuss.*, *10*, 353–391, doi:10.5194/osd-10-353-2013.

Lee, S.-K., W. Park, M. O. Baringer, A. L. Gordon, B. Huber, and Y. Liu (2015), Pacific origin of the abrupt increase in Indian Ocean heat content during the warming hiatus, *Nat. Geosci.*, *8*, 445–449, doi:10.1038/ngeo2438.

Lee, T., I. Fukumori, D. Menemenlis, Z. Xing, and L.-L. Fu (2002), Effects of the Indonesian throughflow on the Pacific and Indian Oceans, *J. Phys. Oceanogr.*, *32*, 1404–1429.

Levang, S. J., and R. W. Schmitt (2015), Centennial changes of the global water cycle in CMIP5 models, *J. Clim.*, doi:10.1175/JCLI-D-15-0143.1.

Masumoto, Y. (2002), Effects of interannual variability in the eastern Indian Ocean on the Indonesian throughflow, *J. Oceanogr.*, *58*(1), 175–182, doi:10.1023/A:1015889004089.

McCreary, J. P., T. Miyama, R. Furue, T. Jensen, H.-W. Kang, B. Bang, and T. Qu (2007), Interactions between the Indonesian Throughflow and circulations in the Indian and Pacific Oceans, *Prog. Oceanogr.*, *75*, 70–114, doi:10.1016/j.pocean.2007.05.004.

McGregor, S., N. J. Holbrook, and S. B. Power (2007), Interdecadal sea surface temperature variability in the equatorial Pacific Ocean. Part I: The role of off-equatorial wind stresses and oceanic Rossby waves, *J. Clim.*, *20*, 2643–2658.

Meijers, A. J. S. (2014), The Southern Ocean in the Coupled Model Intercomparison Project phase 5, *Philos. Trans. R. Soc. London, Ser. A* , *372*, 20130296, doi:10.1098/rsta.2013.0296.

Meyers, G. (1996), Variation of Indonesian throughflow and the El Niño–Southern Oscillation, *J. Geophys. Res.*, *101*, 12,255–12,263, doi:10.1029/95JC03729.

Moss, R. H., et al. (2010), The next generation of scenarios for climate change research and assessment, *Nature*, *463*, 747–756, doi:10.1038/nature08823.

Murtugudde, R., A. J. Busalacchi, and J. Beauchamp (1998), Seasonal-to-interannual effects of the Indonesian throughflow on the tropical Indo-Pacific Basin, *J. Geophys. Res.*, *103*, 21,425–21,441, doi:10.1029/98JC02063.

Oliver, E. C. J., and N. J. Holbrook (2014), Extending our understanding of South Pacific gyre "spin-up": Modeling the East Australian Current in a future climate, *J. Geophys. Res. Oceans*, *119*, 2788–2805, doi:10.1002/2013JC009591.

Roach, A. T., K. Aagaard, C. H. Pease, S. A. Salo, T. Weingartner, V. Pavlov, and M. Kulakov (1995), Direct measurements of transport and water properties through the Bering Strait, *J. Geophys. Res.*, *100*, 18,443–18,457, doi:10.1029/95JC01673.

Roemmich, D., J. Gilson, R. Davis, P. Sutton, S. Wijffels, and S. Riser (2007), Decadal spinup of the South Pacific subtropical gyre, *J. Phys. Oceanogr.*, *37*, 162–173.

Sallée, J.-B., E. Shuckburgh, N. Bruneau, A. J. S. Meijers, T. J. Bracegirdle, Z. Wang, and T. Roy (2013), Assessment of Southern Ocean water mass circulation and characteristics in CMIP5 models: Historical bias and forcing response, *J. Geophys. Res. Oceans*, *118*, 1830–1844, doi:10.1002/jgrc.20135.

Santoso, A., W. Cai, M. H. England, and S. J. Phipps (2011), The role of the Indonesian Throughflow on ENSO dynamics in a coupled climate model, *J. Clim.*, *24*, 585–601, doi:10.1175/2010JCLI3745.1.

Sen Gupta, A., A. Santoso, A. S. Taschetto, C. C. Ummenhofer, J. Trevena, and M. H. England (2009), Projected changes to the Southern Hemisphere ocean and sea ice in the IPCC AR4 climate models, *J. Clim.*, *22*, 3047–3078.

Sen Gupta, A., A. Ganachaud, S. McGregor, J. N. Brown, and L. Muir (2012), Drivers of the projected changes to the Pacific Ocean equatorial circulation, *Geophys. Res. Lett.*, *39*, L09605, doi:10.1029/2012GL051447.

Song, Q., G. A. Vecchi, and A. J. Rosati (2007), The role of the Indonesian Throughflow in the Indo–Pacific climate variability in the GFDL coupled climate model, *J. Clim.*, *20*, 2434–2451, doi:10.1175/JCLI4133.1.

Sprintall, J., and A. Révelard (2014), The Indonesian Throughflow response to Indo-Pacific climate variability, *J. Geophys. Res. Oceans*, 1161–1175, doi:10.1002/2013JC009533.

Sprintall, J., S. E. Wijffels, R. Molcard, and I. Jaya (2009), Direct estimates of the Indonesian Throughflow entering the Indian Ocean: 2004–2006, *J. Geophys. Res.*, *114*, C07001, doi:10.1029/2008JC005257.

Sprintall, J., A. L. Gordon, A. Koch-Larrouy, T. Lee, J. T. Potemra, K. Pujiana, and S. E. Wijffels (2014), The Indonesian seas and their role in the coupled ocean-climate system, *Nat. Geosci.*, *7*, 487–492, doi:10.1038/ngeo2188.

Susanto, R. D., A. L. Gordon, and J. Sprintall (2007), Observations and proxies of the surface layer throughflow in Lombok Strait, *J. Geophys. Res.*, *112*, C03S92, doi:10.1029/2006JC003790.

Swart, N. C., and J. C. Fyfe (2012), Observed and simulated changes in the Southern Hemisphere surface westerly wind-stress, *Geophys. Res. Lett.*, *39*, L16711, doi:10.1029/2012GL052810.

Valsala, V., S. Maksyutov, and R. Murtugudde (2011), Interannual to interdecadal variabilities of the Indonesian Throughflow source water pathways in the Pacific Ocean, *J. Phys. Oceanogr.*, *41*, 1921–1940, doi:10.1175/2011JPO4561.1.

van Sebille, E., M. H. England, J. D. Zika, and B. M. Sloyan (2012), Tasman leakage in a fine-resolution ocean model, *Geophys. Res. Lett.*, *39*, L06601, doi:10.1029/2012GL051004.

Van Sebille, E., J. Sprintall, F. U. Schwarzkopf, A. Sen Gupta, A. Santoso, M. H. England, A. Biastoch, and C. W. Böning (2014), Pacific-to-Indian Ocean connectivity: Tasman leakage, Indonesian Throughflow, and the role of ENSO, *J. Geophys. Res. Oceans*, *119*, 1365–1382, doi:10.1002/2013JC009525.

Wyrtki, K. (1961), Physical oceanography of the Southeast Asian waters, Scripps Institution of Oceanography. [Available at http://escholarship.org/uc/item/49n9x3t4, (Accessed March 30, 2015).]

Yuan, D., H. Zhou, and X. Zhao (2012), Interannual climate variability over the tropical Pacific Ocean Induced by the Indian Ocean dipole through the Indonesian Throughflow, *J. Clim.*, *26*, 2845–2861, doi:10.1175/JCLI-D-12-00117.1.